Science of the Total Environment 907 (2024) 167918

Contents lists available at ScienceDirect

Science of the Total Environment

journal homepage: www.elsevier.com/locate/scitotenv

Interaction of chitosan with nanoplastic in water: The effect of environmental conditions, particle properties, and potential for in situ remediation

Demi T. Djajadi [a,*], Sascha Müller [a,1], Jacek Fiutowski [b], Horst-Günter Rubahn [b], Lisbeth G. Thygesen [a], Nicole R. Posth [a]

[a] Department of Geosciences and Natural Resource Management, University of Copenhagen, DK-1958 Frederiksberg C, Denmark
[b] Mads Clausen Institute, NanoSYD, University of Southern Denmark, DK-6400 Sønderborg, Denmark

HIGHLIGHTS

- Chitosan induced aggregation of nanoplastic across pH, salinity and DOM contents.
- DLS and UV spectrophotometry agreed on chitosan dose for nanoplastic aggregation.
- Nanoplastic removal should not be measured with UV spectrophotometry alone.
- Zeta potential and DLVO calculations partially explain the interaction mechanism.
- Chitosan can be used for in situ aggregation and removal of nanoplastic from water.

GRAPHICAL ABSTRACT

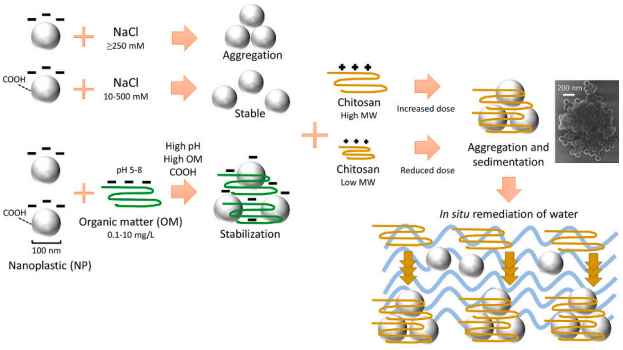

ARTICLE INFO

Editor: Damia Barcelo

Keywords:
Aggregation
Nanoplastic
Chitosan
Environmental conditions
Remediation
Water

ABSTRACT

Micro- and nanoplastic (MNP) pollution in aquatic ecosystems requires investigation on its source, transport, and extent to assess and mitigate its risks. Chitosan is a potential biomolecule for water treatment, but its interaction with MNP is undefined. In this work, chitosan-nanoplastic interaction was explored in the laboratory under environmentally relevant conditions using polystyrene (PS) nanoplastic (NP) as model particle to identify conditions at which PS-chitosan interaction resulted in aggregation. Aggregation limits NP transport and allows separation of NP for targeted remediation. The effect of environmental conditions (pH, salinity, dissolved organic matter (DOM) content), chitosan particle size and NP surface modification on chitosan-NP interaction was studied at various chitosan doses. PS aggregated at chitosan doses as low as 0.2 % *w/w*, while higher doses of chitosan resulted in re-stabilization of NP in solution, restoring the particle size to its initial value. Increasing pH, DOM, or carboxyl modification of the NP surface also improved NP stability in solution. Increased salinity of the

Abbreviations: DLS, dynamic light scattering; DLVO, Derjaguin, Landau, Verwey, Overbeek theory; DOM, dissolved organic matter; DWTP, drinking water treatment plant; EDL, electrical double layer; MNP, micro- and nanoplastics; MP, microplastic; MW, molecular weight; NP, nanoplastic; PAC, poly aluminum chloride; PS, polystyrene; WWTP, waste water treatment plant; ZP, zeta potential.

* Corresponding author.
E-mail address: dtd@ign.ku.dk (D.T. Djajadi).
[1] Present address: Department of Microbial Ecology, Lund University, 223 62 Lund, Sweden.

https://doi.org/10.1016/j.scitotenv.2023.167918
Received 27 July 2023; Received in revised form 21 September 2023; Accepted 16 October 2023
Available online 19 October 2023

solution caused aggregation of unmodified PS independent of chitosan, but carboxyl-modified PS remained stable and aggregated at the same chitosan doses across all salinity levels. Chitosan with low molecular weight promoted PS aggregation at lower doses. Notably, zeta potential (ZP) alone did not indicate chitosan-induced PS aggregation, which occurred independently of changes in ZP. DLVO calculations based on ZP, however, still indicated attractive interaction due to charge differences, albeit with less contrast at high pH, salinity, and DOM content. Additional insights gained in the work recommend caution when using spectrophotometric methods to assess NP removal. Overall, this study demonstrates that chitosan impacts NP transport and holds potential for water remediation of NP.

1. Introduction

Increasing plastic production and consumption coupled with material cycle mismanagement has led to accumulating plastic debris in the environment at an unprecedented scale. About 19–23 Mt. plastic waste entered aquatic ecosystems in 2016, and the rate might double by 2030 despite current mitigations (Borrelle et al., 2020). Abiotic and biotic processes in the environment fragment plastic debris into smaller particles, i.e., microplastic (MP, 1 to <1000 μm) and nanoplastic (NP, 1 to <1000 nm) (Gigault et al., 2018; Hartmann et al., 2019). The small size of micro- and nanoplastics (MNP) increase their distribution in the environment, and they are readily transported and ingested by various organisms in aquatic ecosystems (Athey et al., 2020; Rogers et al., 2020). Studies on model organisms (Bhagat et al., 2021) and human cells (Shi et al., 2022), among others indicate MNP toxicity. Furthermore, MNP act as vectors of heavy metals and persistent organic pollutants (Alimi et al., 2018), making remediation approaches vital.

Remediation of MNP already takes place in waste water treatment plants (WWTP), which removes larger MP efficiently (10–100 μm), but fails to sufficiently target the smaller NP (Krishnan et al., 2023; Ma et al., 2019; Zhang et al., 2020). Filtration processes in WWTP can be hindered by MNP due to clogging and abrasion of membrane filters, resulting in fragmentation of MNP into even smaller particles that pass through the filters to discharge into waterways (Enfrin et al., 2019). NP presents potentially higher ecological and health risks than MP due to their small size, colloidal nature and high surface area to volume ratio (Cai et al., 2021). The extent of NP pollution in the environment, however, remains poorly defined, as detection and quantification methods are still under development. Nevertheless, NP is likely thought to be more abundant and broadly distributed than MP and engineered nanoparticles in the environment due to large amount of plastic waste produced globally and their small size (Sharma et al., 2023). Thus, developing novel methods targeting NP remediation in aquatic environments is crucial. One option towards this goal employs aggregation and settling of NP in situ to limit further transport and uptake in the food chain.

There have been several studies on the coagulation and flocculation of model NP, especially using metal salts within WWTP or drinking water treatment plants (DWTP). The conventional coagulant poly aluminum chloride (PAC) has shown some potential in removing PS NP either through coagulation alone (Gong et al., 2022; Zhang et al., 2022) or in combination with other processes at DWTP, e.g. sand filtration and granular activated carbon (Hofman-Caris et al., 2022; Ramirez Arenas et al., 2022, 2020). Other metal-organic particles with Cu—Ni (Zhou et al., 2022) and Fe (Jung et al., 2023) also have NP removal potential. However, using metal coagulants, especially aluminum, has potential adverse health and environmental effects (Gauthier et al., 2000; Peydayesh et al., 2019) and is thus unsuitable for in situ remediation in aquatic ecosystems. Organic and biological coagulants are better suited for remediation purposes as they can be directly applied in water bodies, although this approach has not been widely explored (Tang et al., 2022). Recently, several works using biomolecules, e.g. protein and natural gum (González-Monje et al., 2021), jellyfish mucin (Ben-David et al., 2023), and starch (Hu et al., 2023) have shown the possibility for NP aggregation, capture and removal. Hence, finding potential biomolecules that are abundant and able to induce NP aggregation is an important step towards achieving in situ remediation.

Chitosan is derived from the environmentally abundant chitin, a polysaccharide found in arthropods, invertebrates, fungi and some microbes. It is non-toxic and biodegradable and is readily available as a by-product of the shellfish industry (Synowiecki and Al-Khateeb, 2003). It has long been studied as a promising bio-based flocculants for water purification (Lichtfouse et al., 2019; Yang et al., 2016). Chitosan has also been used as a component in membrane filtration (Risch and Adlhart, 2021), as a gel-based adsorbent (Zheng et al., 2022) and for multi-component coagulation together with tannic acid and iron (III) (Park et al., 2023) as well as with PAC (Huang et al., 2023) to remove MP from water. Hence, we hypothesize that chitosan can be utilized for in situ water remediation of NP through aggregation and sedimentation.

To date, only one study on the interaction of chitosan with model sulfate-modified PS MP has been conducted, finding that adding chitosan increased and eventually inverted the zeta potential (ZP) of PS (Ramirez et al., 2016). This observation was used to indicate aggregation, yet actual particle size measurement was absent. Herein, we systematically investigate the interaction between chitosan and PS NP under background physicochemical conditions reflecting fresh/groundwater, brackish water, and seawater. PS NP interactions with chitosan in water at various doses, pH, salinity, and DOM content were studied during batch aggregation experiments. The resulting aggregates were assessed for their spectrophotometric, hydrodynamic and electrokinetic properties to identify the driving factors for aggregation between PS NP and chitosan. By studying the effect of biomolecules on NP transport, this work outlines a potential method for in situ water remediation through aggregation of NP as well as highlights the roles of particle properties and environmental factors in NP transport.

2. Materials and methods

2.1. Polymers and chemicals

PS with no surface modification (PS-Plain) and carboxyl-modified surface (PS-COOH), both with 100 nm diameter were purchased from Micromod Partikeltechnologie GmbH (Rostock, Germany) acted as models for NP. PS-COOH acted as a proxy of plastic after UV-induced photo-oxidation, since plastics exposed to UV reveal surface carboxyl groups (Gewert et al., 2018). Chitosan with low (50–190 kDa, ≥75 % deacetylation) and high (310–375 kDa, ≥75 % deacetylation) molecular weight (MW), and sodium alginate from brown algae were purchased from Sigma-Aldrich (St. Louis, MO, USA). Glacial acetic acid, sodium chloride (NaCl), 37 % *w/w* hydrochloric acid (HCl), potassium hydroxide (KOH) and sodium bicarbonate ($NaHCO_3$) were purchased from Sigma-Aldrich (St. Louis, MO, USA). The stock solutions of PS-Plain and PS-COOH (1000 mg/L) were prepared in deionized water. Chitosan stock solutions (500 mg/L) were prepared by dissolving chitosan in 1 % *v/v* acetic acid. Alginate stock solution (500 mg/L) was prepared by dissolving alginate in deionized water.

2.2. Aggregation experiments and assessment

The pH (5, 6.5, 8) and salinity levels (10, 250, 500 mM NaCl or 0.58, 14.6, 29.2 ‰) were chosen to reflect conditions in different aquatic

environments, i.e. fresh/groundwater, brackish water, and seawater, respectively (Appelo and Postma, 2005; Yao and Byrne, 2001). Sodium alginate of 1, 10, 100 % *w/w* (0.1, 1, 10 mg/L) were used to test the effect of increasing DOM content on chitosan-NP interaction. This range represents DOM content in aquatic environments (Alimi et al., 2022; Li et al., 2019; Oriekhova and Stoll, 2018; Wu et al., 2019). The effect of these environmental conditions on the aggregation of PS-Plain and PS-COOH was studied using low MW (LMW) and high MW (HMW) chitosan over a dose range of 0.1–100 % *w/w* (0.001–10 mg/L). The concentration of PS NP in the experiments was 10 mg/L, which is higher than expected in the environment, but enables accurate detection and is similar to the concentrations used in other studies (Mao et al., 2020; Pradel et al., 2021; Zhang et al., 2019). Unless otherwise specified, the aggregation experiments were performed in batches of 5 mL volume in 10 mM NaCl at pH 5 and ambient temperature (21 ± 1 °C). This base case was chosen as conditions where the performance of chitosan is not limited by deprotonation (Yang et al., 2016) and the aggregation of PS NP is not affected by high salinity alone (Dong et al., 2020; Shams et al., 2020). The solution pH was adjusted using HCl, KOH and $NaHCO_3$ to reach the initial pH of 5, 6.5 and 8, respectively. The solutions were filtered through a 0.2 μm filter before adding PS NP and biomolecules. The experiments were performed in 15 mL test tubes positioned horizontally on an orbital shaker and mixed at 150 RPM for 20 min followed by centrifugation at 2000*g* for 1 min. The experimental duration was chosen based on static aggregation experiments where the increase in PS NP size reached equilibrium after around 20 min (Fig. S1). Three experimental replicates were performed.

Afterwards, the PS NP colloidal suspension was characterized for extent of aggregation and particle size. Sample aliquots (0.4 mL) were taken from the solution surface and measured in a UV cuvette to indicate PS NP aggregation by reading the absorbance at 225 nm using an Epoch 2 spectrophotometer (BioTek Instruments, Inc., Winooski, VT, USA). At this wavelength, both PS NP had maximum absorbance (Figs. S2 & S3), whereas the biomolecules had minimum absorbance at the tested concentrations (Fig. S4). Aggregation was reported as C/C_0, where C and C_0 indicate the absorbance of PS NP after and prior to the experiment, respectively. The hydrodynamic diameter of PS NP was measured using a dynamic light scattering (DLS) instrument (NANO-flex II) with a 785 nm laser and 180° backscattering angle (Colloid Metrix GmbH, Meersbusch, Germany).

2.3. Measurement of zeta potential

The zeta potential (ZP) of the particles was measured using Stabino II (Colloid Metrix GmbH, Meersbusch, Germany), which is based on streaming potential and the Smoluchowski model. The 0.4 mm gap size piston was used on the standard measurement cell with a 10 mL reaction volume. ZP was measured separately from DLS in selected conditions of the aggregation experiments, i.e., the doses near the point of apparent maximum aggregation, and using only HMW chitosan. Time-resolved ZP measurements were conducted over 30 min with 5 min intervals of 12 readings each. Two experimental replicates were performed.

2.4. DLVO interaction energy calculation

The interaction energy of PS NP and chitosan under various experimental conditions was calculated using ZP measurement results and based on DLVO (Derjaguin, Landau, Verwey, Overbeek) theory. The method is outlined in Text S1.

2.5. Microscopy imaging

The PS NP and the aggregates of selected conditions were prepared using the same experimental setups, but at a ten-fold higher PS NP, chitosan and alginate concentrations. The samples were visualized under an Orion NanoFAB He-ion microscope (Carl Zeiss, Oberkochen, Germany). The beam energy was 30 keV, with a probe current ranging from 0.05 to 0.1 pA. The advantage of this method is that samples do not need conductive coatings. The samples were drop-casted from a liquid solution to a piece of silicon substrate 1–100 Ω/1 cm^2. There was no charge compensation needed to perform the imaging. However, a cross-check with a low-energy electron beam, a flood gun at 433 eV, was performed against unwanted charging effects. Images were taken from 8 to 10 randomly selected spots distributed over 5 × 5 mm^2 sample area on each sample.

3. Results and discussion

3.1. Effect of pH on the chitosan-induced aggregation of PS NP

The apparent optimum chitosan dose for PS NP aggregation, as seen in the increase of size (hydrodynamic diameter) and concomitant decrease of C/C_0, differed between the pH values and the PS NP type (Fig. 1). Surface modification resulted in a four to tenfold higher chitosan dose required to achieve aggregation of PS-COOH than PS-Plain. Nevertheless, both PS-Plain and PS-COOH aggregates reduced in size with a concomitant increase of C/C_0 at higher chitosan doses in all cases (Fig. 1). This was likely a re-stabilization of the neutralized flocs due to excess cationic charge when overdosing chitosan (Lichtfouse et al., 2019). Minor variations in C/C_0 (ca. 0–0.2) at chitosan doses where PS NP did not aggregate are likely due to spectrophotometer sensitivity/detection limit and/or occlusion of PS NP by chitosan. When increasing pH, higher chitosan doses were required to aggregate both PS-Plain and PS-COOH, approximately two-fold from pH 5 to 6.5 and four-fold from pH 5 to 8 (Fig. 1). This was expected as the charge of chitosan, a weak cationic polyelectrolyte, depends on the pH value. At lower pH, chitosan is more protonated and interacts more strongly with other particles of contrasting charge, among others via a charge neutralization effect (Lichtfouse et al., 2019; Yang et al., 2016). The ZP of HMW chitosan was accordingly reduced from 24.5 ± 1.6 mV at pH 5 to 10.1 ± 3 mV and −3.7 ± 2.2 mV at pH 6.5 and 8, respectively (Fig. 2). This reduction of chitosan ZP at higher pH has also been seen previously (Ramirez et al., 2016).

The ZP of PS-Plain and PS-COOH increased with chitosan dose, but decreased with higher pH and reached equilibrium after around 20 min for all pH values (Fig. 2). The charge inversion at pH 5 and 6.5 (Fig. 1 A-B, D-E) can be explained by the increasing dose of positively-charged chitosan at low pH (Fig. 2) (Lichtfouse et al., 2019; Yang et al., 2016). At pH 8, charge inversion was less apparent in experiments with PS-Plain and almost disappeared in PS-COOH (Fig. 1 C & F). Increasing pH reduces the charge difference between chitosan and PS, and the energy spectrum expresses a reduced electrical double layer (EDL). DLVO calculations still indicate attractive forces at pH 8, albeit lower than at pH 5 and 6.5 (Fig. 3 A). This causes the interaction between PS NP and chitosan to occur near particle surface (under 50 nm distance) at pH 8. At pH 5, however, the reactive boundary moves further away from the particle surface (up to 150 nm) (Fig. 3 A) leading to a higher likelihood of adsorption and aggregation (Fig. 1 A & D). At pH > 8, other aggregation mechanisms can be more dominant for chitosan, e.g., a sweeping effect where precipitating chitosan forms an enmeshing network that traps the pollutants despite losing its positive charge (Blockx et al., 2018).

A ZP of 0 mV has been used to indicate aggregation in chitosan-PS MP interaction, although no size measurement of these aggregates was reported (Ramirez et al., 2016). In this work, ZP reaching 0 mV and eventual charge inversion at pH 5 and 6.5 (Fig. 2 A-B, D-E) was not found to coincide with PS NP aggregation. Aggregation occurred at HMW chitosan doses of 0.5 and 1 % *w/w* for PS-Plain at pH 5 and 6.5, respectively (Fig. 1 A & D) and at 5 and 10 % *w/w* for PS-COOH at pH 5 and 6.5, respectively (Fig. 1 B & E). In these cases, the ZP at which aggregation occurred was around −20 to −10 mV. At pH 8, there was no charge inversion, and the ZP of PS-COOH barely changed even at 20 %

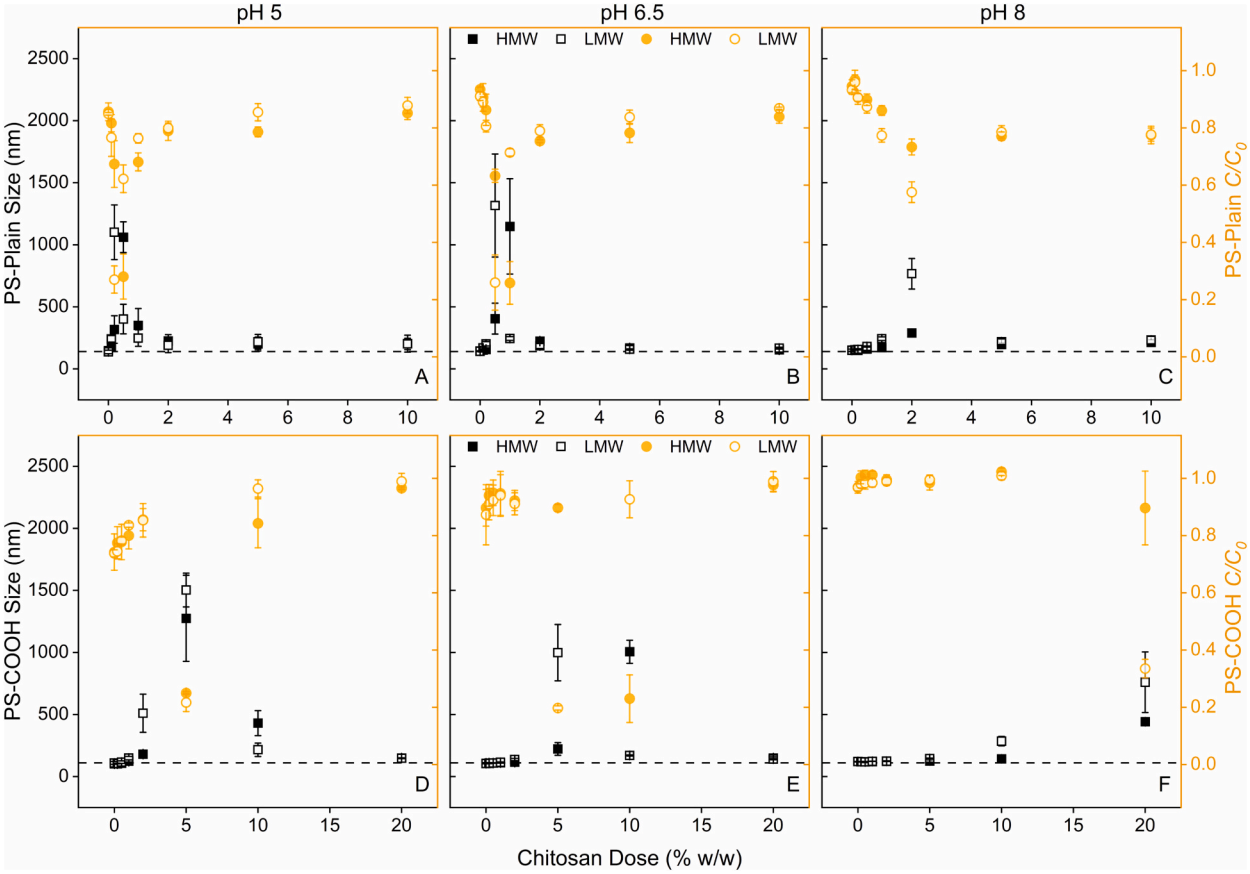

Fig. 1. Aggregation of PS-Plain (A-C) and PS-COOH (D-F) with high (HMW) and low (LMW) molecular weight (MW) chitosan at initial pH 5 (A and D), 6.5 (B and E), 8 (C and F) at various chitosan doses (% *w/w*) as presented by hydrodynamic diameter (left-axis) and C/C_0 (right-axis). The salinity in all experiments was 10 mM NaCl. The horizontal dashed lines mark the initial hydrodynamic diameter of PS-Plain (140 nm) and PS-COOH (110 nm). Data points are averages and standard deviations of three replicates.

w/w chitosan dose (Fig. 2 C & F). Yet, there was aggregation at chitosan doses of 2 % *w/w* with PS-Plain (Fig. 1 C) and 20 % *w/w* with PS-COOH (Fig. 1 F). Thus, ZP was not a good indicator of aggregation, while the combined use of ZP and DLS was essential.

3.2. *Effect of salinity on the chitosan-induced aggregation of PS NP*

For PS-Plain, there was an apparent optimum chitosan dose required for aggregation at low salinity (10 mM NaCl), but aggregation occurred regardless of chitosan dose at high salinity levels (Fig. 4 A-C). The aggregates of PS-Plain at ≥250 mM NaCl are in the order of several micrometers, which is at the limit of DLS (6.5 μm) (Bhattacharjee, 2016), hence causing major standard deviation (Fig. 4 B-C). Regardless, the individual data points still indicate PS-Plain aggregation due to high salinity level irrespective of chitosan dose. Again, surface modification was crucial, as PS-COOH aggregation occurred only at certain doses of chitosan (2 and 5 % *w/w*) and remained similar across all salinity levels (Fig. 4 D-F). This can be somewhat expected as higher NaCl concentration (CCC) was required to achieve the aggregation of PS-COOH than PS-Plain (Wang et al., 2020), and PS-COOH showed higher stability than PS-Plain in the presence of various salts (Wu et al., 2019; Zhang et al., 2019). Overdosing of chitosan at various salinity levels also re-stabilized PS-Plain and PS-COOOH, and the size increase was accompanied by a decrease of C/C_0 (Fig. 4 A-F).

ZP values of both PS-Plain and PS-COOH reached close to 0 mV at high salinity (Fig. 5 B-C, E-F). This explains the aggregation behavior of PS-Plain at high salinity (Fig. 4 B-C), but not PS-COOH (Fig. 4 E-F). For PS-Plain, the EDL is reduced with increasing salt concentration, as the ZP is minimized and only attractive van der Waals forces persist. Thus, DLVO forces (Fig. 3 B) can explain PS-Plain aggregation. No difference between 250 and 500 mM NaCl is seen because the CCC of PS-Plain is likely exceeded already at 250 mM NaCl, causing no further effect on the EDL. However, DLVO forces do not explain the ZP of PS-COOH, as aggregation occurred only at certain doses (Fig. 4 E & F), while ZP remained close to 0 mV throughout. Hence, ZP did not indicate PS-COOH aggregation as is similar to findings in the pH experiments (Figs. 1 & 2). Steric forces induced by COOH groups are not represented in the DLVO forces. DLVO theory predicts aggregation for PS-COOH similar to PS-Plain (Fig. 3 B), yet the experimental data clearly shows no overall aggregation (Fig. 4 D-F). This indicates that the steric effects of COOH groups prevent NP aggregation. As a consequence, the presence of strong steric forces (via i.e., high density of COOH groups) invalidates the previous understanding that ionic strength beyond the CCC causes rapid aggregation of NP (Shams et al., 2020; Singh et al., 2019; Wu et al., 2019).

3.3. *Effect of DOM content on the chitosan-induced aggregation of PS NP*

Higher DOM content increased the chitosan dose needed for aggregation of both PS NP (Fig. 6). For PS-Plain, the required chitosan dose increased five-fold from 1 to 10 % *w/w* DOM and ten-fold from 10 to 100 % *w/w* DOM (Fig. 6 A-C). In contrast, for PS-COOH, the corresponding increase was about two-fold and six-fold, respectively (Fig. 6 D-F). Control experiments showed that alginate did not reduce the UV absorbance of PS NP up to 1:1 *w/w* ratio (Fig. S5), and the presence of alginate without chitosan (0 % *w/w* dose) did not increase PS NP size even at 100 % *w/w* DOM content (Fig. 6). Aggregates were not detected by He-ion microscopy, unlike when chitosan was present at apparent

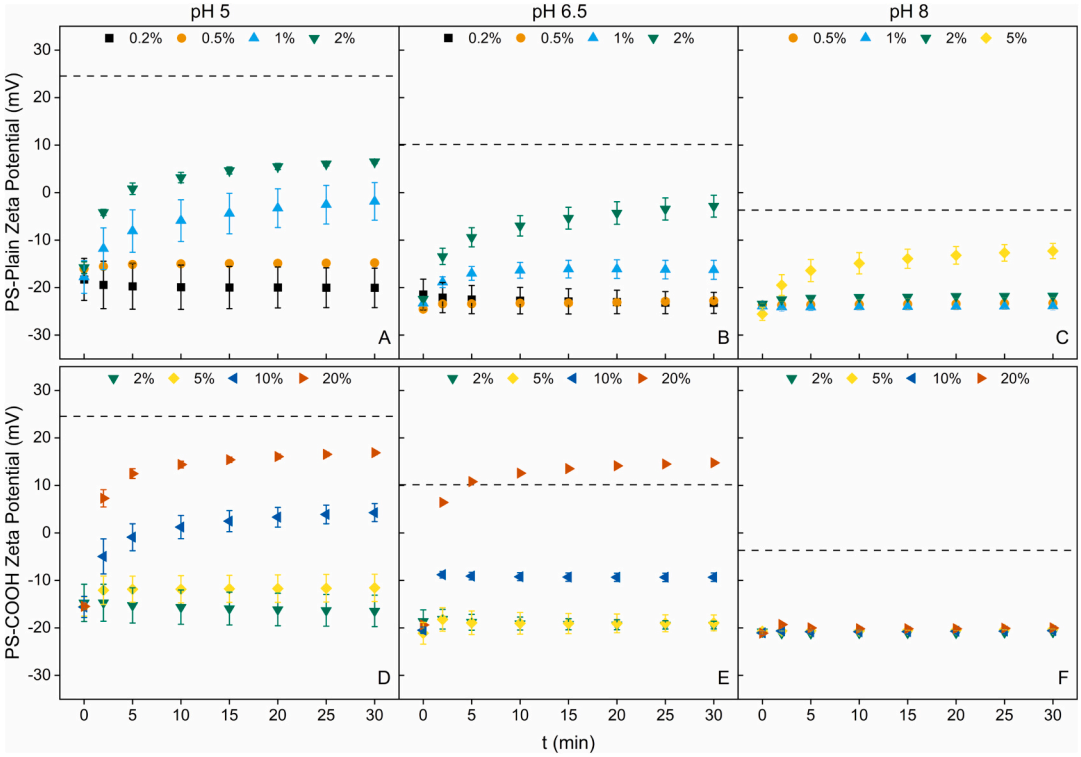

Fig. 2. Zeta potential (ZP) of PS-Plain (A-C) and PS-COOH (D-F) with high molecular weight (HMW) chitosan at initial pH 5 (A and D), 6.5 (B and E), 8 (C and F) at various chitosan doses (% *w/w*). The salinity in all experiments was 10 mM NaCl. The horizontal dashed lines mark the ZP of 10 mg/L HMW chitosan at pH 5 (24.5 mV), 6.5 (10.1 mV) and 8 (−3.7 mV). Data points are averages and standard deviations of two replicates.

optimum dose with or without alginate (Fig. 7). Hence, the reduction of C/C_0 and increase of PS NP aggregate size cannot be attributed to PS NP-alginate interaction alone.

The presence of DOM (i.e., humic substances) is known to stabilize PS NP of similar charge, mainly due to steric repulsion, even in conditions which could otherwise lead to aggregation (Li et al., 2019; Shams et al., 2020; Wu et al., 2019). This stabilization was observed in the ZP of both PS NP with increasing alginate content and chitosan dose. Higher alginate content resulted in slightly lower ZP and higher chitosan dose required to achieve charge inversion of both PS-Plain and PS-COOH (Fig. 8) than when alginate was absent (Fig. 2). In order to better understand this, DLVO interaction energy was calculated from the ZP of both PS-Plain and PS-COOH in the presence of fixed alginate content (10 % *w/w* or 1 mg/L) with increasing chitosan dose (2, 20, 100 % *w/w* or 0.2, 2, 10 mg/L). It shows that in the presence of DOM, low chitosan dose formed a repulsive layer as chitosan charge was inverted, hence alginate prevented PS NP-chitosan aggregation. However, there was no charge inversion at higher chitosan dose, and DLVO indicates attractive forces (Fig. 3 C). Nevertheless, as in the previous cases (Figs. 2 & 5), changes in ZP values in the presence of DOM (Fig. 8) did not indicate aggregation.

At the highest DOM content (1:1 *w/w* of PS NP and alginate), almost an equal amount of chitosan (5–10 mg/L) was needed to induce PS NP aggregation (Fig. 6 C & F). A significant amount of pellets was produced after centrifugation, especially for HMW chitosan, which was not observed at lower doses (Fig. S6). One possible explanation is that aggregation at high DOM content also occurred due to chitosan-alginate interaction, forming an encapsulating/enmeshing layer. Indeed chitosan and alginate have been used as combined polyelectrolyte complexes as drug carriers (Li et al., 2009) and artificial tissue scaffolds (Venkatesan et al., 2014). Sodium alginate itself stabilizes NP via encapsulation and bridging (Alimi et al., 2022; Pradel et al., 2021). Thus, it is likely that alginate-chitosan interaction results in aggregation and sedimentation of NP as also indicated by He-ion microscopy (Fig. 7). Accordingly, the ZP of alginate was inverted when about 1:1 *w/w* chitosan dose was applied in the absence of PS NP (Fig. S7). The interaction of two biomolecules has indeed been proposed as a potential method to clean water from nano-sized contaminants through encapsulation (González-Monje et al., 2021). This also implies that using chitosan to clean water of NP can remove other pertinent organic materials and pollutants.

3.4. *Effect of PS modification on the chitosan-induced aggregation of PS NP*

The chitosan dose needed to induce aggregation of PS-COOH was generally higher (up to twenty-fold) than PS-Plain at varying pH and DOM contents (Figs. 1 & 6). At seawater salinity level, the carboxyl groups stabilized PS NP in solution, making chitosan necessary for aggregation (Fig. 4). The presence of hydrophilic carboxyl groups (in PS-COOH) provide repulsive short-ranged steric and hydration forces pertaining to the particle surface (Notley and Norgren, 2006), and prevent adsorption. No repulsive force is seen in the DLVO plot, but the EDL is reduced to 25–50 nm (Fig. 3). Therefore, near the particle surface at pH 8, the repulsive forces may reach beyond the compressed EDL, overruling the weak charge difference and preventing adsorption. However, this component is not accounted for in DLVO, and therefore can only be speculated. In any case, this condition can be overcome by increasing the chitosan dose (Fig. 1), which increases the likelihood of collision and attachment.

UV-irradiation of plastic results in the scission of bonds and exposure of surface carboxyl groups (Gewert et al., 2018; Wang et al., 2020), which leads to improved NP stability in the presence of salt (Mao et al., 2020). Accordingly, studies comparing model NP with and without carboxyl groups surface modification also showed better stability of the former in solutions of increasing salt concentration (Müller et al., 2021; Wang et al., 2020). Therefore, as NP is subject to weathering processes in the environment, they will have exposed carboxyl groups on the surface.

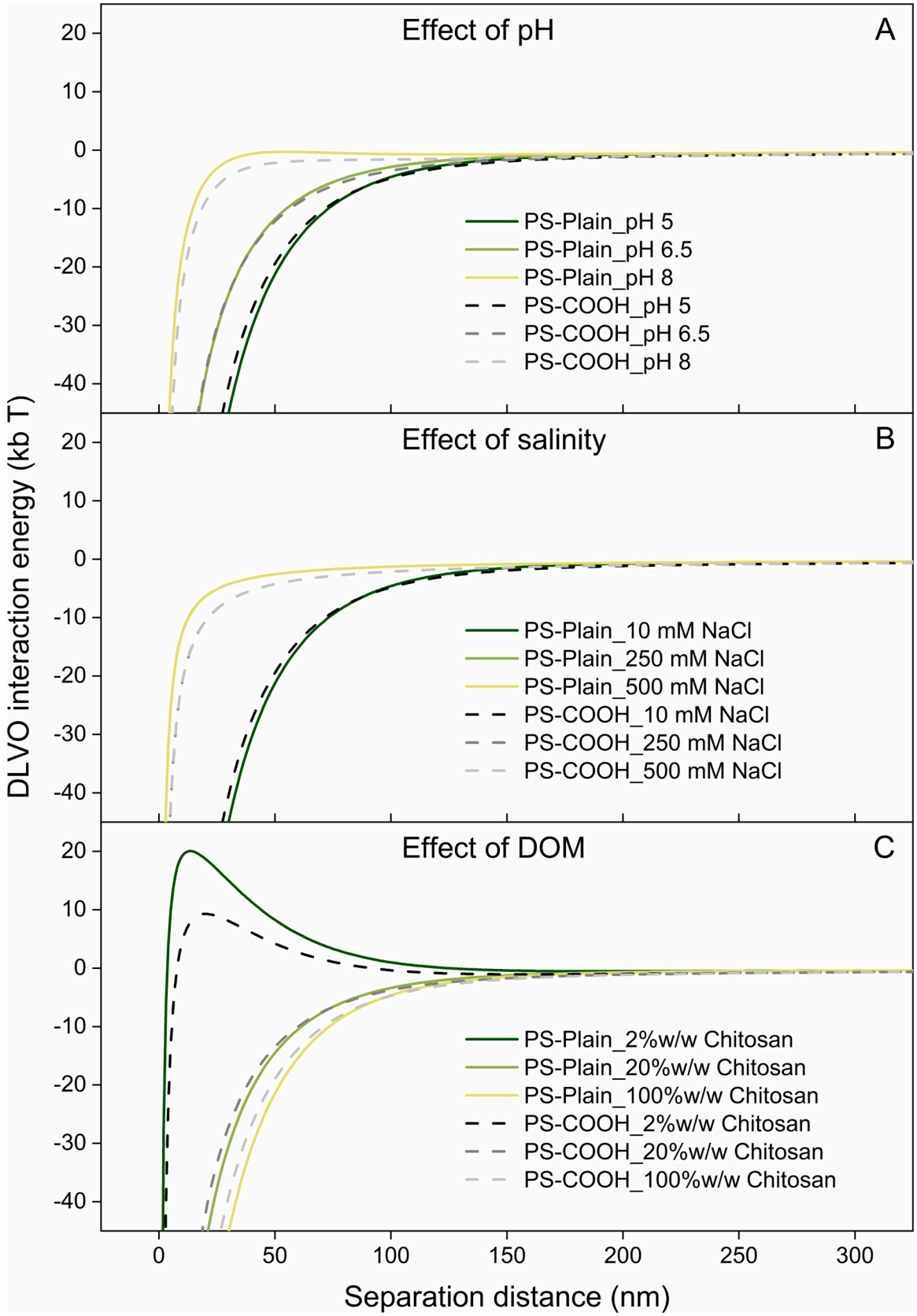

Fig. 3. DLVO interaction energy plot for PS NP-chitosan interaction accounting for van der Waals and electrical double layer (EDL) forces at various pH values (A), salinity levels (B), and in the presence of DOM (1 mg/L alginate). The calculation was based on the zeta potential of PS NP and HMW chitosan at the respective conditions.

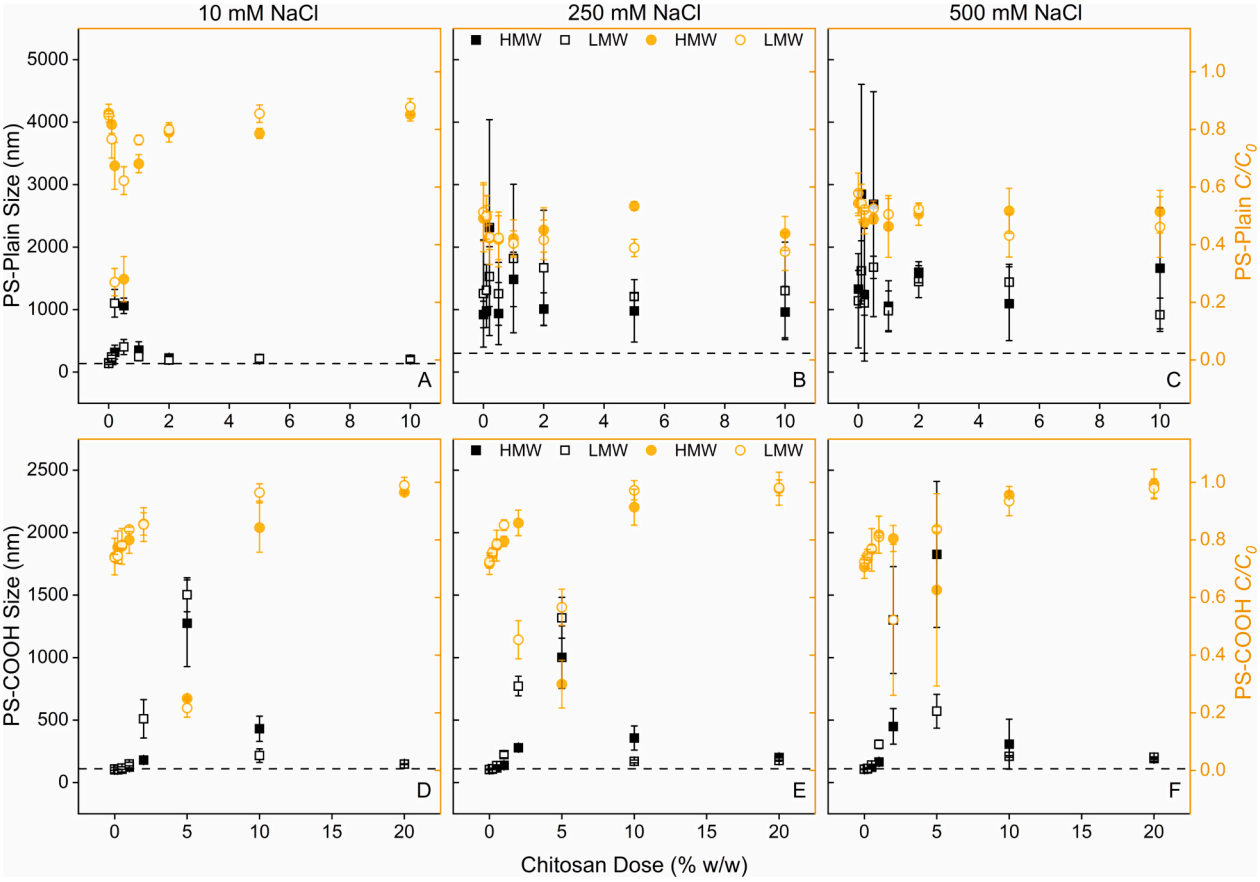

Fig. 4. Aggregation of PS-Plain (A-C) and PS-COOH (D-F) with high (HMW) and low (LMW) molecular weight (MW) chitosan in various salinity levels, i.e., 10 mM NaCl (A and D), 250 mM NaCl (B and E), 500 mM NaCl (C and F) at various chitosan doses (% *w/w*) as presented by hydrodynamic diameter (left-axis) and C/C_0 (right-axis). The initial pH of all experiments was 5. The horizontal dashed lines mark the initial hydrodynamic diameter of PS-Plain (140 nm at 10 mM NaCl, 300 nm at 250 and 500 mM NaCl) and PS-COOH (110 nm). Data points are averages and standard deviations of three replicates.

This suggests improved stability and further transport of NP, even in brackish and saline environments such as estuaries and oceans. Hence, a remediation approach using chitosan will be relevant across multiple aquatic environments. However, NP in the environment can also interact with suspended sediments (Laursen et al., 2023; Li et al., 2019) and microorganisms (Rogers et al., 2020), affecting their surface properties and transport behavior. For example, MP has been shown to flocculate with natural fine-grained sediments (Andersen et al., 2021; Laursen et al., 2023) and in saline environments, therefore accumulating in estuaries (Laursen et al., 2023). Assuming NP behaves similarly, using chitosan to capture and limit NP transport in rivers can prevent its accumulation in saline environments.

3.5. *Effect of chitosan MW on the chitosan-induced aggregation of PS NP*

Generally, a lower amount (ca. 50 %) of LMW chitosan was needed to cause aggregation of both PS-Plain and PS-COOH (Figs. 1, 4, 6) compared to HMW chitosan. This is quite the opposite of what was expected from previous studies, where higher MW flocculants performed more efficiently than lower MW flocculants (Djajadi et al., 2022; Wickramasinghe et al., 2010). However, reports for chitosan diverge (Yang et al., 2016) as several works showed that LMW chitosan performed more efficiently than HMW chitosan, i.e., it flocculated faster at lower doses (Meraz et al., 2016; Strand et al., 2002). In those works, however, the degree of acetylation was different, which can also affect coagulation-flocculation (Yang et al., 2016). As LMW and HMW chitosans in this work have similar degree of acetylation, a possible explanation could be that there were more LMW chitosan molecules than HMW chitosan molecules at the same dose based on weight.

3.6. *Assessment of NP aggregation*

In assessing NP aggregation, DLS is a widely used tool to measure the size increase (Oriekhova and Stoll, 2018; Pradel et al., 2021; Ramirez et al., 2016; Shams et al., 2020; Wu et al., 2019). Additionally, UV–Vis spectrophotometry is used to monitor aggregation of engineered nanoparticles in aquatic environments (Praetorius et al., 2020). Accordingly in this study, an overall agreement was found in chitosan-NP aggregation as assessed by DLS and UV spectrophotometry, i.e., an increase in hydrodynamic diameter was followed by a reduction of C/C_0 (Figs. 1, 4, 6). However, in recent works studying NP removal from water using various coagulants and processes (Hofman-Caris et al., 2022; Park et al., 2023; Zhang et al., 2022; Zhou et al., 2022), the reduction of UV absorbance or fluorescence intensity was used as an indicator of NP removal. It is rather tempting and straightforward to do so, as concentration of PS NP has a linear correlation with UV absorbance (Figs. S2 & S3). Hence, one can calculate the percentage of NP removal by calculating the reduction of UV absorbance or fluorescence intensity. Yet as this study shows, a reduction in UV absorbance can also indicate adsorption and aggregation. Therefore, caution is needed, as using UV spectrophotometry as the sole indicator of NP removal can be misleading as it cannot distinguish between adsorption, aggregation and removal of the particles. Even greater caution is needed when using model fluorescent NP, as aggregation-induced quenching (reduction of fluorescence intensity due to binding) and dye leakage might also affect fluorescent intensity (Andreiuk et al., 2019).

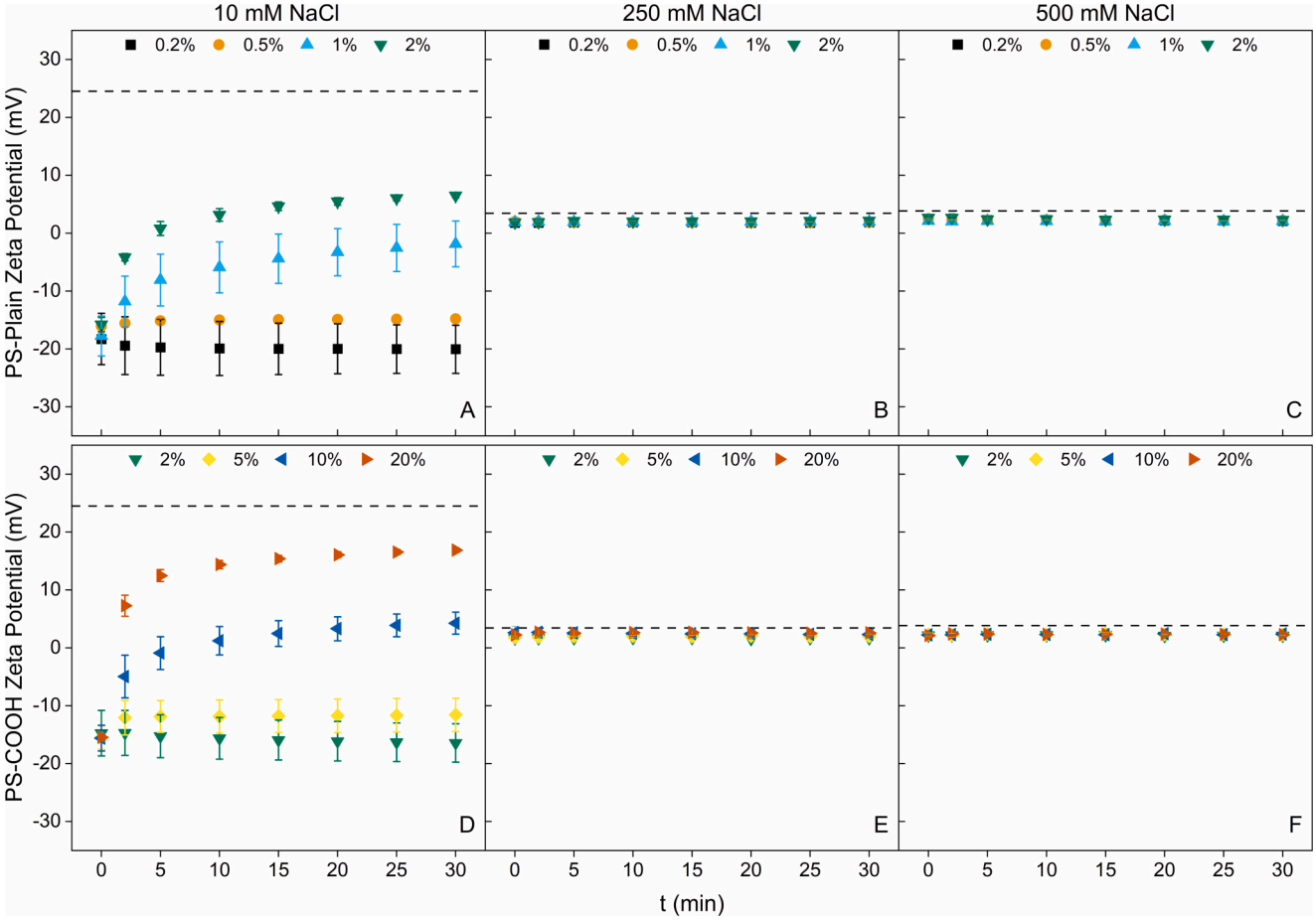

Fig. 5. Zeta potential (ZP) of PS-Plain (A-C) and PS-COOH (D-F) with high molecular weight (HMW) chitosan at salinity of 10 mM NaCl (A and D), 250 mM NaCl (B and E), 500 mM NaCl (C and F) at various chitosan doses (% *w/w*). The initial pH in all experiments was 5. The horizontal dashed lines mark the ZP of 10 mg/L HMW chitosan at 10 mM NaCl (24.5 mV), 250 mM NaCl (3.4 mV) and 500 mM NaCl (3.9 mV). Data points are averages and standard deviations of two replicates.

ZP was measured in this study because it has been conventionally used within WWTP as an indicator of the optimal coagulation-flocculation condition (or accomplished charge neutralization) at a narrow window of ZP around 0 mV (Henderson et al., 2008; Morfesis et al., 2009). The only previous work using chitosan indicated the point of PS MP coagulation as the chitosan dose and conditions at which ZP value reached zero and inverted (Ramirez et al., 2016). In this work, the ZP data (Figs. 2, 5, 8) did not directly indicate the dose at which maximum aggregation occurred in the test system, except for PS-Plain at high salinity (Fig. 4 B & C). Aggregation mostly occurred (Figs. 1, 4, 6) when ZP was similar to the initial value before chitosan addition or before it was inverted (Figs. 2, 5, 8). Hence, ZP cannot under all conditions be used as the sole indicator of aggregation when studying MNP-biomolecule interactions. Other studies on the interaction between NP with minerals and/or DOM found ZP to be close to 0 mV when aggregation occurred, as seen in an increase in hydrodynamic diameter (Oriekhova and Stoll, 2018; Ramirez Arenas et al., 2020), while others showed no aggregation despite inverted or low ZP (Wu et al., 2019; Zhang et al., 2019). Therefore, it is likely that ZP can indicate MNP aggregation under certain conditions, but not necessarily always at a narrow window of ZP close to 0 mV or when it is inverted. It is also important to note that ZP itself can be affected by various factors such as pH, ionic strength and particle concentration (Bhattacharjee, 2016).

3.7. Perspectives on potential water remediation of NP using chitosan

Aggregation of NP induced by chitosan means that it can potentially be used for remediation by limiting NP transport or capturing and separating NP. In this work, a dose as low as 0.2 % *w/w* increased the size of 100 nm PS NP to >1000 nm (Fig. 1). In another study, 0.8 % *w/w* jellyfish mucus (based on total protein) increased the size of 100 nm PS NP to ca. 600 nm, while the corresponding increase for chemical flocculants was ca. 800 nm with 0.4 % *w/w* $FeCl_3$ and ca. 600 nm with 2 % *w/w* PAC (Ben-David et al., 2023). Hence, chitosan has potential to be used in a wide array of remediation applications, although it is a technical challenge to avoid overdosing, which can re-stabilize the aggregates in the solution (Figs. 1, 4 & 6) (Lichtfouse et al., 2019). The size increase of PS NP from 100 nm to ≥1 μm (Figs. 1, 4 & 6) is large enough to promote aggregation and sedimentation of NP as seen with direct visual inspection (Fig. S6) and microscopy (Fig. 7). From an engineering perspective, it enables sedimentation of the otherwise colloidal NP and importantly decreases the filtration range needed from ultrafiltration (0.01–0.1 μm) to microfiltration (0.1–10 μm), which facilitates removal. However, the actual remediation setup remains to be adjusted to the target conditions, but filtration of the aggregated NP followed by biological degradation in an enclosed compartment (e.g., a container or vessel) could be one possibility. Alternatively, chitosan can be formulated as an adsorbent capable of several regeneration cycles (Risch and Adlhart, 2021; Wang et al., 2021; Zheng et al., 2022).

From an environmental perspective, using chitosan for in situ NP capture and removal should ideally be performed in an enclosed compartment. Otherwise, by promoting aggregation of NP to MP-size or larger, NP aggregates can be expected to behave as MP, i.e., flocculating to the bottom of water bodies with natural sediments and organic matter, which increases NP loading to the benthic zone (Laursen et al., 2023, 2022). This is not an ideal remediation process as it still exposes

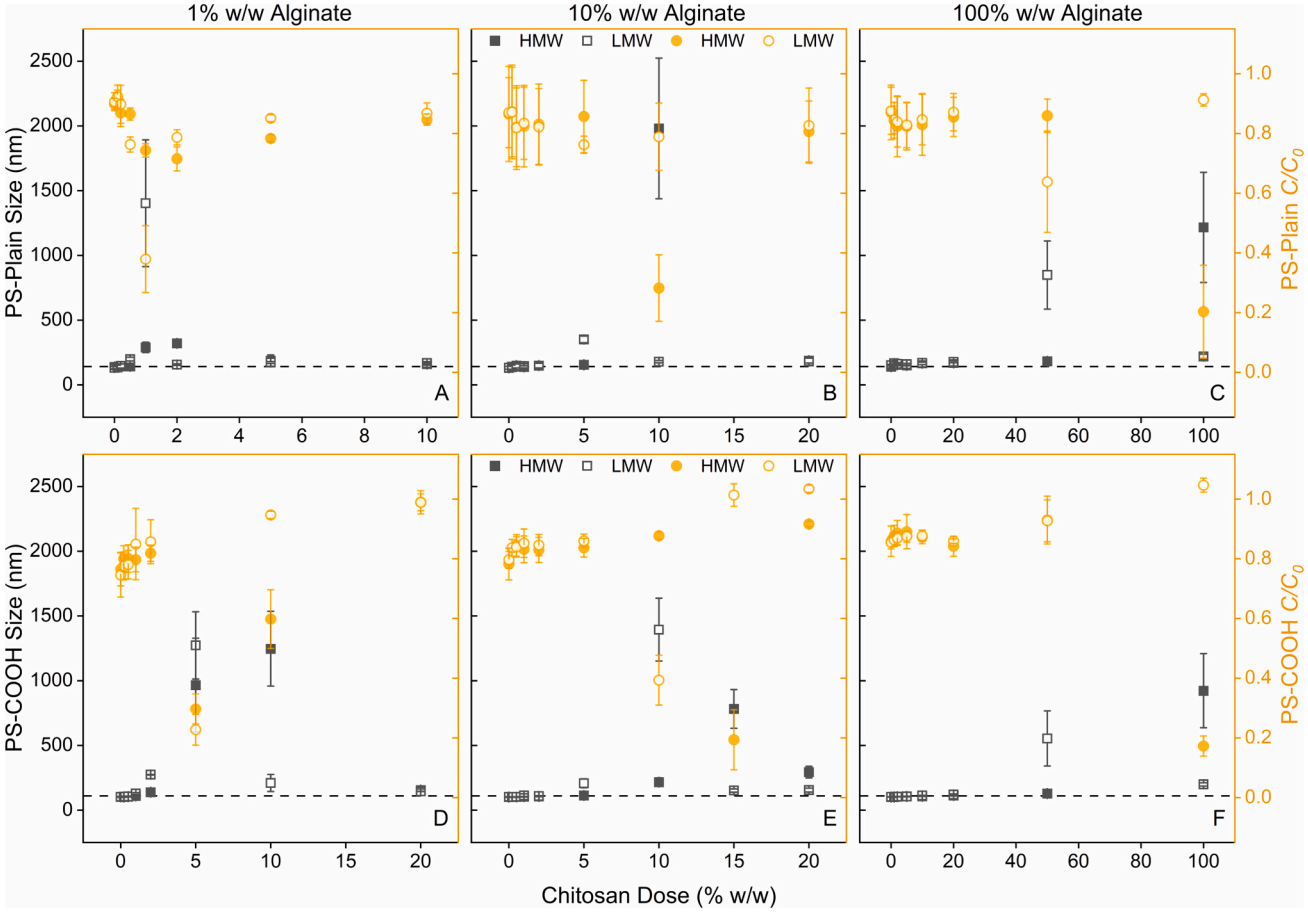

Fig. 6. Aggregation of PS-Plain (A-C) and PS-COOH (D-F) with high (HMW) and low (LMW) molecular weight (MW) chitosan at DOM (alginate) content of 1 % *w/w* (A and D), 10 % *w/w* (B and E), 100 % *w/w* (C and F) at various chitosan doses (% *w/w*) as presented by hydrodynamic diameter (left-axis) and C/C_0 (right-axis). The initial pH of all experiments was 5 and the salinity was 10 mM NaCl. The horizontal dashed lines mark the initial hydrodynamic diameter of PS-Plain (140 nm) and PS-COOH (110 nm). Data points are averages and standard deviations of three replicates.

biota to MNP and even risks uptake into the food chain. However, mimicking this natural process using biomolecules in an enclosed compartment allows environmental-friendly NP removal. Even if the aggregation and sedimentation of NP is performed directly without enclosed compartment, this approach allows limiting contaminant transport by "immobilizing" NP, especially if future risk assessments deem NP to be a hazardous pollutant of high risk. It is still important as the colloidal nature of NP suggests enhanced transport than MP, even when aggregated or forming "eco-corona" with particular biomolecules (Dong et al., 2020; Li et al., 2021). In this case, biomolecules promoting aggregation and limiting transport could be beneficial.

Concerning environmental conditions and particle properties, this study shows the ability of chitosan to induce aggregation of model PS NP across pH, salinity and DOM content as well as with COOH surface modification as UV-degradation proxy (Figs. 1, 4 & 6). Although all factors (except salinity) increased NP stability in solution, increased chitosan dose can still induce NP aggregation (Fig. S8). DOM content is likely to play a larger role in the environment than the other factors as it greatly outnumbers the amount of NP in nature, up to 10,000:1 (Alimi et al., 2022). The highest ratio of DOM to NP (1:1) used in this study is thus unrealistically low, but still higher than others (Tallec et al., 2019; Wu et al., 2019). Nevertheless, until sensitive NP detection is developed and the extent of NP pollution is well-known, the flocculant needs to be able to interact with DOM to facilitate removal. To this point, chitosan has high potential.

4. Conclusions

Chitosan-nanoplastic interaction under relevant background physicochemical aquatic ecosystem conditions showed that chitosan can affect nanoplastic aggregation and transport, and has potential to be utilized in remediation approaches. The key findings in this study are:

- Chitosan can induce the aggregation of model polystyrene nanoplastic at a certain window of apparent optimal dose, as low as 0.2 % *w/w*.
- Higher pH and dissolved organic matter content of the water, and carboxyl surface modification of polystyrene nanoplastic increased its stability in the solution and accordingly also increased the chitosan dose required to achieve aggregation.
- The influence of salinity strongly depends on nanoplastic surface. Aggregation of unmodified polystyrene at increased salinity occurred independently of chitosan doses. In contrast, carboxyl-modified polystyrene remained stable and aggregated at the same chitosan doses across all salinity levels.
- Chitosan with low molecular weight required less dose to induce nanoplastic aggregation than the high molecular weight chitosan, generally by a factor of two.
- This work also highlights the need for caution when using both spectrophotometric and zeta potential measurements in studying nanoplastic interaction and removal. Spectrophotometric data cannot be used as sole indicator of nanoplastic removal. Change of

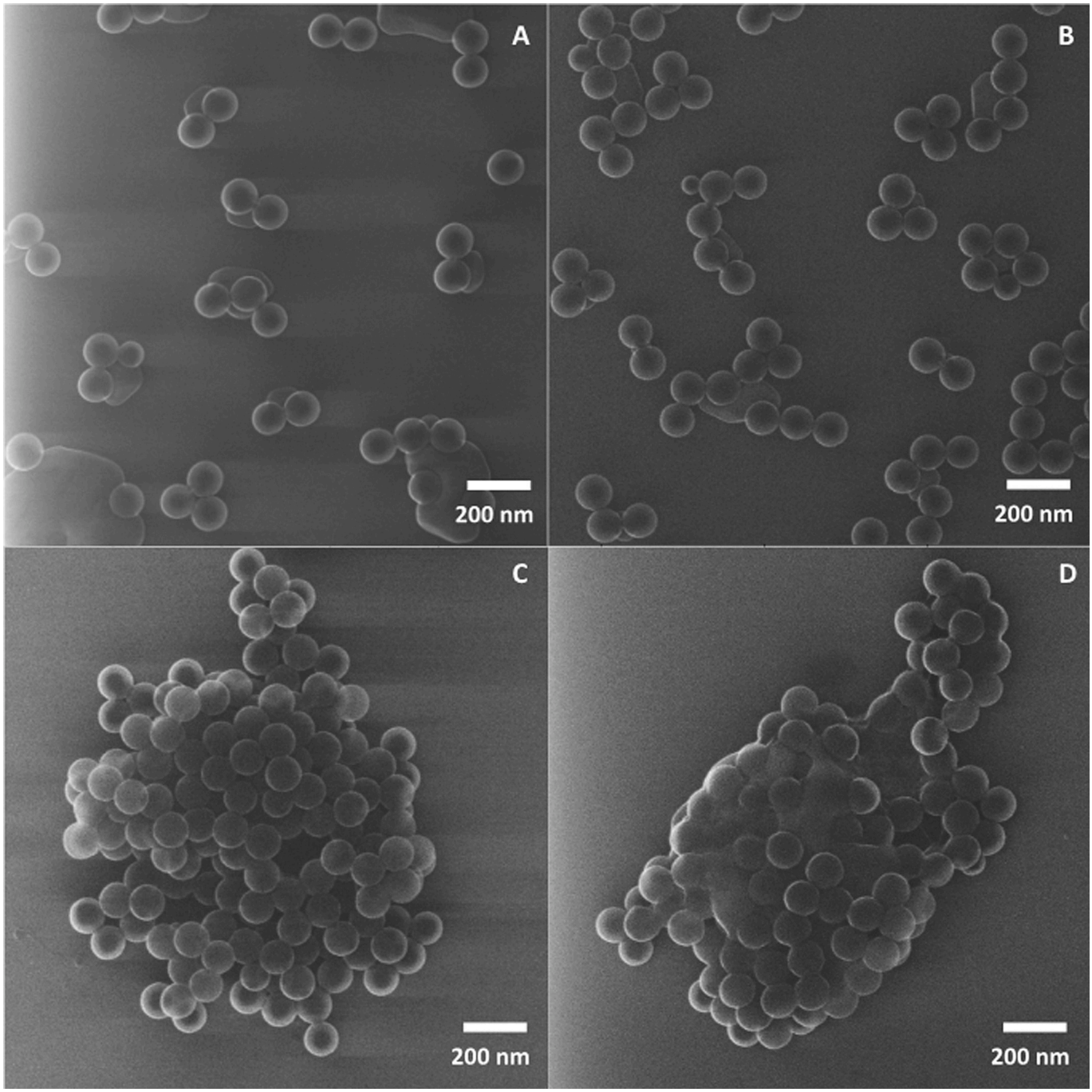

Fig. 7. He-ion microscopy images of PS-Plain (A), PS-Plain in the presence of 10 % *w/w* alginate (B), PS-Plain aggregate at optimum HMW chitosan dose of 0.5 % *w/w* (C), and PS-Plain aggregate at 10 % *w/w* alginate and optimum HMW chitosan dose of 10 % *w/w* (D). All experiments were performed in 10 mM NaCl at pH 5, and PS-Plain concentration of 100 mg/L.

zeta potential to 0 mV cannot be used as sole indicator of nanoplastic aggregation.

Further aspects of this work remain to be explored in future studies. First, more environmentally relevant nanoplastic should be used instead of the model pristine spherical particles. Second, additional biomolecules can be explored in two key ways: 1) those abundant in particular environments to understand their effect on the fate and transport of micro- and nanoplastic, and 2) those with potential as bio-based flocculants. In that respect, chitosan as a removal agent can be further improved, modified, and studied for its effect on the toxicity of micro- and nanoplastic and other pertaining contaminants. Last, actual in situ remediation methods can be developed, provided that these preliminary laboratory findings prove to be relevant in actual environmental settings.

CRediT authorship contribution statement

Demi T. Djajadi: Conceptualization, Methodology, Investigation, Writing – original draft, Funding acquisition, Visualization, Writing – review & editing. **Sascha Müller:** Formal analysis, Methodology, Visualization, Writing – review & editing. **Jacek Fiutowski:** Investigation, Visualization, Writing – review & editing. **Horst-Günter Rubahn:** Investigation, Visualization, Writing – review & editing. **Lisbeth G.**

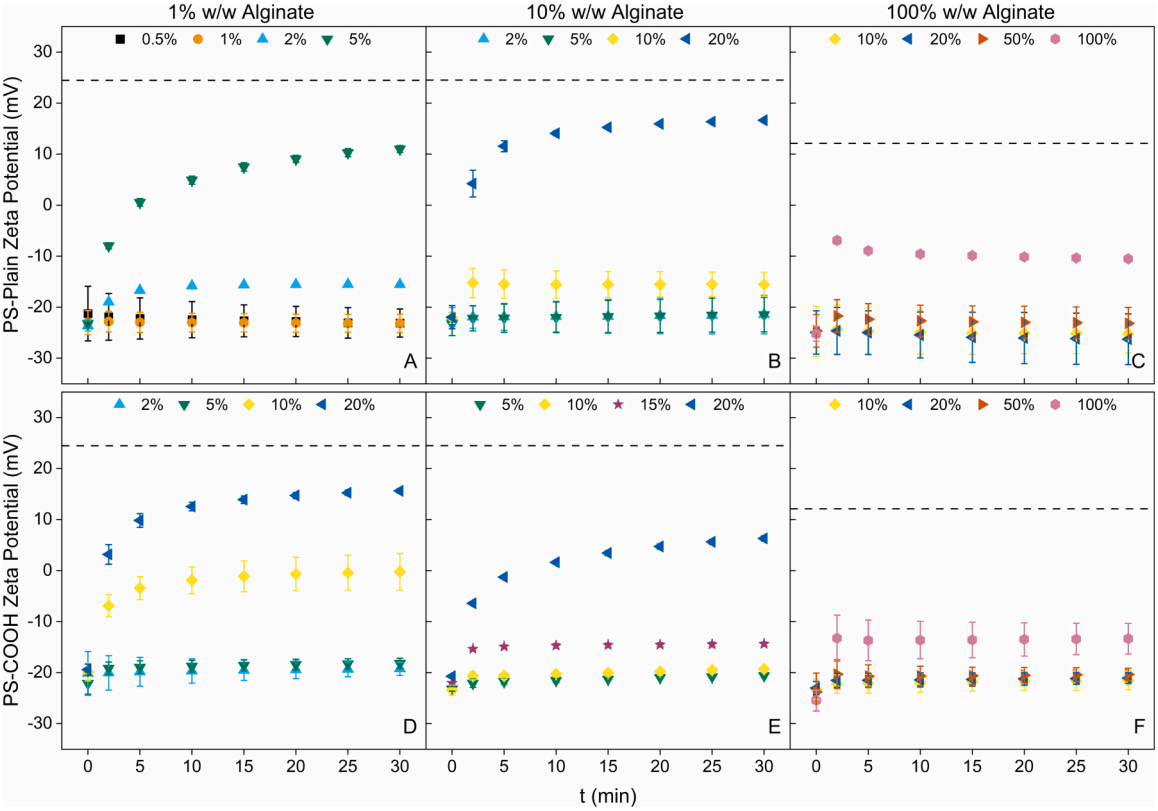

Fig. 8. Zeta potential (ZP) of PS-Plain (A-C) and PS-COOH (D-F) with high molecular weight (HMW) chitosan at DOM (alginate) content of 1 % *w/w* (A and D), 10 % *w/w* (B and E), 100 % *w/w* (C and F) at various chitosan doses (% *w/w*). The initial pH in all experiments was 5 and the salt concentration was 10 mM NaCl. The horizontal dashed lines mark the ZP of 10 mg/L HMW chitosan with 1 % *w/w* alginate (24.5 mV), 10 % *w/w* alginate (24.5 mV) and 100 % *w/w* alginate (12.1 mV). Data points are averages and standard deviations of two replicates.

Thygesen: Formal analysis, Supervision, Writing – review & editing. **Nicole R. Posth:** Supervision, Resources, Writing – review & editing.

Declaration of competing interest

The authors declare that they have no known competing financial interests or personal relationships that could have appeared to influence the work reported in this paper.

Data availability

Data will be made available on request.

Acknowledgements

This work was supported by VILLUM FONDEN (grant number 40950). The microscopy imaging was supported by Interreg 6a Deutschland-Danmark Program under project PlastTrack (grant number 07-1-22 1). Associate Professor Søren Jessen is acknowledged for discussion on water chemistry.

Appendix A. Supplementary data

Supplementary data to this article can be found online at https://doi.org/10.1016/j.scitotenv.2023.167918.

References

Alimi, O.S., Farner Budarz, J., Hernandez, L.M., Tufenkji, N., 2018. Microplastics and nanoplastics in aquatic environments: aggregation, deposition, and enhanced contaminant transport. Environ. Sci. Technol. 52, 1704–1724. https://doi.org/10.1021/acs.est.7b05559.

Alimi, O.S., Farner, J.M., Rowenczyk, L., Petosa, A.R., Claveau-Mallet, D., Hernandez, L. M., Wilkinson, K.J., Tufenkji, N., 2022. Mechanistic understanding of the aggregation kinetics of nanoplastics in marine environments: comparing synthetic and natural water matrices. J. Hazard. Mater. Adv. 7, 100115 https://doi.org/10.1016/j.hazadv.2022.100115.

Andersen, T.J., Rominikan, S., Olsen, I.S., Skinnebach, K.H., Fruergaard, M., 2021. Flocculation of PVC microplastic and fine-grained cohesive sediment at environmentally realistic concentrations. Biol. Bull. 240, 42–51. https://doi.org/10.1086/712929.

Andreiuk, B., Reisch, A., Bernhardt, E., Klymchenko, A.S., 2019. Fighting aggregation-caused quenching and leakage of dyes in fluorescent polymer nanoparticles: universal role of counterion. Chem. Asian J. 14, 836–846. https://doi.org/10.1002/asia.201801592.

Appelo, C.A.J., Postma, D., 2005. Geochemistry, Groundwater and Pollution, 2nd ed. A. A. Balkema, Leiden.

Athey, S.N., Albotra, S.D., Gordon, C.A., Monteleone, B., Seaton, P., Andrady, A.L., Taylor, A.R., Brander, S.M., 2020. Trophic transfer of microplastics in an estuarine food chain and the effects of a sorbed legacy pollutant. Limnol. Oceanogr. Lett. 5, 154–162. https://doi.org/10.1002/lol2.10130.

Ben-David, E.A., Habibi, M., Haddad, E., Sammar, M., Angel, D.L., Dror, H., Lahovitski, H., Booth, A.M., Sabbah, I., 2023. Mechanism of nanoplastics capture by jellyfish mucin and its potential as a sustainable water treatment technology. Sci. Total Environ. 869, 161824 https://doi.org/10.1016/j.scitotenv.2023.161824.

Bhagat, J., Nishimura, N., Shimada, Y., 2021. Toxicological interactions of microplastics/nanoplastics and environmental contaminants: current knowledge and future perspectives. J. Hazard. Mater. 405, 123913 https://doi.org/10.1016/j.jhazmat.2020.123913.

Bhattacharjee, S., 2016. DLS and zeta potential - what they are and what they are not? J. Control. Release 235, 337–351. https://doi.org/10.1016/j.jconrel.2016.06.017.

Blockx, J., Verfaillie, A., Thielemans, W., Muylaert, K., 2018. Unravelling the mechanism of chitosan-driven flocculation of microalgae in seawater as a function of pH. ACS Sustain. Chem. Eng. 6, 11273–11279. https://doi.org/10.1021/acssuschemeng.7b04802.

Borrelle, S.B., Ringma, J., Law, K.L., Monnahan, C.C., Lebreton, L., McGivern, A., Murphy, E., Jambeck, J., Leonard, G.H., Hilleary, M.A., Eriksen, M., Possingham, H. P., Rochman, C.M., 2020. Mitigate plastic pollution. Science (80-.) 1518, 1515–1518.

Cai, H., Xu, E.G., Du, F., Li, R., Liu, J., Shi, H., 2021. Analysis of environmental nanoplastics: progress and challenges. Chem. Eng. J. 410, 128208 https://doi.org/10.1016/j.cej.2020.128208.

Djajadi, D.T., Brenelli, L.B., Franco, T.T., Thygesen, L.G., Jørgensen, H., 2022. Lignosulfonate properties and reaction conditions enhance precipitation and affect ensuing quality of proteins from green biomass juice for monogastric animal feed. Anim. Feed Sci. Technol. 285, 115212 https://doi.org/10.1016/j.anifeedsci.2022.115212.

Dong, Z., Hou, Y., Han, W., Liu, M., Wang, J., Qiu, Y., 2020. Protein corona-mediated transport of nanoplastics in seawater-saturated porous media. Water Res. 182, 115978 https://doi.org/10.1016/j.watres.2020.115978.

Enfrin, M., Dumée, L.F., Lee, J., 2019. Nano/microplastics in water and wastewater treatment processes – origin, impact and potential solutions. Water Res. 161, 621–638. https://doi.org/10.1016/j.watres.2019.06.049.

Gauthier, E., Fortier, I., Courchesne, F., Pepin, P., Mortimer, J., Gauvreau, D., 2000. Aluminum forms in drinking water and risk of Alzheimer's disease. Environ. Res. 84, 234–246. https://doi.org/10.1006/enrs.2000.4101.

Gewert, B., Plassmann, M., Sandblom, O., Macleod, M., 2018. Identification of chain scission products released to water by plastic exposed to ultraviolet light. Environ. Sci. Technol. Lett. 5, 272–276. https://doi.org/10.1021/acs.estlett.8b00119.

Gigault, J., ter Halle, A., Baudrimont, M., Pascal, P.Y., Gauffre, F., Phi, T.L., El Hadri, H., Grassl, B., Reynaud, S., 2018. Current opinion: what is a nanoplastic? Environ. Pollut. 235, 1030–1034. https://doi.org/10.1016/j.envpol.2018.01.024.

Gong, Y., Bai, Y., Zhao, D., Wang, Q., 2022. Aggregation of carboxyl-modified polystyrene nanoplastics in water with aluminum chloride: structural characterization and theoretical calculation. Water Res. 208, 117884 https://doi.org/10.1016/j.watres.2021.117884.

González-Monje, P., Ayala García, A., Ruiz-Molina, D., Roscini, C., 2021. Encapsulation and sedimentation of nanomaterials through complex coacervation. J. Colloid Interface Sci. 589, 500–510. https://doi.org/10.1016/j.jcis.2020.12.067.

Hartmann, N.B., Hüffer, T., Thompson, R.C., Hassellöv, M., Verschoor, A., Daugaard, A. E., Rist, S., Karlsson, T., Brennholt, N., Cole, M., Herrling, M.P., Hess, M.C., Ivleva, N. P., Lusher, A.L., Wagner, M., 2019. Are we speaking the same language? Recommendations for a definition and categorization framework for plastic debris. Environ. Sci. Technol. 53, 1039–1047. https://doi.org/10.1021/acs.est.8b05297.

Henderson, R.K., Parsons, S.A., Jefferson, B., 2008. Successful removal of algae through the control of zeta potential. Sep. Sci. Technol. 43, 1653–1666. https://doi.org/10.1080/01496390801973771.

Hofman-Caris, C.H.M., Bäuerlein, P.S., Siegers, W.G., Mintenig, S.M., Messina, R., Dekker, S.C., Bertelkamp, C., Cornelissen, E.R., van Wezel, A.P., 2022. Removal of nanoparticles (both inorganic nanoparticles and nanoplastics) in drinking water treatment - coagulation/flocculation/sedimentation, and sand/granular activated carbon filtration. Environ. Sci. Water Res. Technol. 8, 1675–1686. https://doi.org/10.1039/d2ew00226d.

Hu, P., Sun, Y., Li, P., Ren, W., Ren, J., Su, K., Cai, J., El-Sayed, M.M.H., Shoeib, T., Yang, H., 2023. Evaluation of the nanoplastics removal by using starch-based coagulants: roles of the chain architecture and hydrophobicity of the coagulant. Sep. Purif. Technol. 319, 124045 https://doi.org/10.1016/j.seppur.2023.124045.

Huang, L., He, W., Zhang, Y., Wang, X., Wu, K., Yang, Z., Zhang, J., 2023. Chitosan enhances poly aluminum chloride flocculation system removal of microplastics: effective, stable, and pollution free. J. Water Process Eng. 54, 103929 https://doi.org/10.1016/j.jwpe.2023.103929.

Jung, Y., Yoon, S., Byun, J., Jung, K., Choi, J., 2023. Visible-light-induced self-propelled nanobots against nanoplastics. Water Res. 244, 120543 https://doi.org/10.1016/j.watres.2023.120543.

Krishnan, R.Y., Manikandan, S., Subbaiya, R., Karmegam, N., Kim, W., Govarthanan, M., 2023. Recent approaches and advanced wastewater treatment technologies for mitigating emerging microplastics contamination – a critical review. Sci. Total Environ. 858, 159681 https://doi.org/10.1016/j.scitotenv.2022.159681.

Laursen, S.N., Fruergaard, M., Andersen, T.J., 2022. Rapid flocculation and settling of positively buoyant microplastic and fine-grained sediment in natural seawater. Mar. Pollut. Bull. 178, 113619 https://doi.org/10.1016/j.marpolbul.2022.113619.

Laursen, S.N., Fruergaard, M., Dodhia, M.S., Posth, N.R., Rasmussen, M.B., Larsen, M.N., Shilla, Dativa, Shilla, Daniel, Kilawe, J.J., Kizenga, H.J., Andersen, T.J., 2023. Settling of buoyant microplastic in estuaries: the importance of flocculation. Sci. Total Environ. 886, 163976 https://doi.org/10.1016/j.scitotenv.2023.163976.

Li, X., Xie, H., Lin, J., Xie, W., Ma, X., 2009. Characterization and biodegradation of chitosan-alginate polyelectrolyte complexes. Polym. Degrad. Stab. 94, 1–6. https://doi.org/10.1016/j.polymdegradstab. 2008.10.017.

Li, Y., Wang, X., Fu, W., Xia, X., Liu, C., Min, J., Zhang, W., Crittenden, J.C., 2019. Interactions between nano/micro plastics and suspended sediment in water: implications on aggregation and settling. Water Res. 161, 486–495. https://doi.org/10.1016/j.watres.2019.06.018.

Li, X., He, E., Xia, B., Liu, Y., Zhang, P., Cao, X., Zhao, L., Xu, X., Qiu, H., 2021. Protein corona-induced aggregation of differently sized nanoplastics: impacts of protein type and concentration. Environ. Sci. Nano 8, 1560–1570. https://doi.org/10.1039/d1en00115a.

Lichtfouse, E., Morin-Crini, N., Fourmentin, M., Zemmouri, H., do Carmo Nascimento, I. O., Queiroz, L.M., Tadza, M.Y.M., Picos-Corrales, L.A., Pei, H., Wilson, L.D., Crini, G., 2019. Chitosan for direct bioflocculation of wastewater. Environ. Chem. Lett. 17, 1603–1621. https://doi.org/10.1007/s10311-019-00900-1.

Ma, B., Xue, W., Ding, Y., Hu, C., Liu, H., Qu, J., 2019. Removal characteristics of microplastics by Fe-based coagulants during drinking water treatment. J. Environ. Sci. (China) 78, 267–275. https://doi.org/10.1016/j.jes.2018.10.006.

Mao, Y., Li, H., Huangfu, X., Liu, Y., He, Q., 2020. Nanoplastics display strong stability in aqueous environments: insights from aggregation behaviour and theoretical calculations. Environ. Pollut. 258, 113760 https://doi.org/10.1016/j.envpol.2019.113760.

Meraz, K.A.S., Vargas, S.M.P., Maldonado, J.T.L., Bravo, J.M.C., Guzman, M.T.O., Maldonado, E.A.L., 2016. Eco-friendly innovation for nejayote coagulation-flocculation process using chitosan: evaluation through zeta potential measurements. Chem. Eng. J. 284, 536–542. https://doi.org/10.1016/j.cej.2015.09.026.

Morfesis, A., Jacobson, A.M., Frollini, R., Helgeson, M., Billica, J., Gertig, K.R., 2009. Role of zeta (ζ) potential in the optimization of water treatment facility operations. Ind. Eng. Chem. Res. 48, 2305–2308. https://doi.org/10.1021/ie800524x.

Müller, S., Fiutowski, J., Rubahn, H.-G., Posth, N.R., 2021. Nanoplastic transport in aqueous environments: the role of chemo-electric properties and hydrodynamic forces for nanoplastic-mineral interaction. ChemRxiv Preprint. https://doi.org/10.26434/chemrxiv-2021-zcv78.

Notley, S.M., Norgren, M., 2006. Measurement of interaction forces between lignin and cellulose as a function of aqueous electrolyte solution conditions. Langmuir 22, 11199–11204. https://doi.org/10.1021/la0618566.

Oriekhova, O., Stoll, S., 2018. Heteroaggregation of nanoplastic particles in the presence of inorganic colloids and natural organic matter. Environ. Sci. Nano 5, 792–799. https://doi.org/10.1039/c7en01119a.

Park, J.W., Jin, Lee, Su, Jin, Y.J., Jeon, Y., Lee, Seon Jae, Kim, Y., Kwon, G., Hwang, D.Y., Seo, S., 2023. Phenolic-modified cationic polymers as coagulants for microplastic removal. J. Ind. Eng. Chem. 119, 208–217. https://doi.org/10.1016/j.jiec.2022.11.039.

Peydayesh, M., Pauchard, M., Bolisetty, S., Stellacci, F., Mezzenga, R., 2019. Ubiquitous aluminium contamination in water and amyloid hybrid membranes as a sustainable possible solution. Chem. Commun. 55, 11143–11146. https://doi.org/10.1039/c9cc05337a.

Pradel, A., Ferreres, S., Veclin, C., El Hadri, H., Gautier, M., Grassl, B., Gigault, J., 2021. Stabilization of fragmental polystyrene nanoplastic by natural organic matter: insight into mechanisms. ACS EST Water 1, 1198–1208. https://doi.org/10.1021/acsestwater.0c00283.

Praetorius, A., Badetti, E., Brunelli, A., Clavier, A., Gallego-Urrea, J.A., Gondikas, A., Hassellöv, M., Hofmann, T., Mackevica, A., Marcomini, A., Peijnenburg, W., Quik, J. T.K., Seijo, M., Stoll, S., Tepe, N., Walch, H., Von Der Kammer, F., 2020. Strategies for determining heteroaggregation attachment efficiencies of engineered nanoparticles in aquatic environments. Environ. Sci. Nano 7, 351–367. https://doi.org/10.1039/c9en01016e.

Ramirez Arenas, L., Ramseier Gentile, S., Zimmermann, S., Stoll, S., 2020. Coagulation of TiO2, CeO2 nanoparticles, and polystyrene nanoplastics in bottled mineral and surface waters. Effect of water properties, coagulant type, and dosage. Water Environ. Res. 92, 1184–1194. https://doi.org/10.1002/wer.1313.

Ramirez Arenas, L., Ramseier Gentile, S., Zimmermann, S., Stoll, S., 2022. Fate and removal efficiency of polystyrene nanoplastics in a pilot drinking water treatment plant. Sci. Total Environ. 813, 152623 https://doi.org/10.1016/j.scitotenv.2021.152623.

Ramirez, L., Gentile, S.R., Zimmermann, S., Stoll, S., 2016. Comparative study of the effect of aluminum chloride, sodium alginate and chitosan on the coagulation of polystyrene micro-plastic particles. J. Colloid Sci. Biotechnol. 5, 190–198. https://doi.org/10.1166/jcsb.2016.1149.

Risch, P., Adlhart, C., 2021. A chitosan nanofiber sponge for oyster-inspired filtration of microplastics. ACS Appl. Polym. Mater. 3, 4685–4694. https://doi.org/10.1021/acsapm.1c00799.

Rogers, K.L., Carreres-Calabuig, J.A., Gorokhova, E., Posth, N.R., 2020. Micro-by-micro interactions: how microorganisms influence the fate of marine microplastics. Limnol. Oceanogr. Lett. 5, 18–36. https://doi.org/10.1002/lol2.10136.

Shams, M., Alam, I., Chowdhury, I., 2020. Aggregation and stability of nanoscale plastics in aquatic environment. Water Res. 171, 115401 https://doi.org/10.1016/j.watres.2019.115401.

Sharma, V.K., Ma, X., Lichtfouse, E., Robert, D., 2023. Nanoplastics are potentially more dangerous than microplastics. Environ. Chem. Lett. 21, 1933–1936. https://doi.org/10.1007/s10311-022-01539-1.

Shi, Q., Tang, J., Liu, R., Wang, L., 2022. Toxicity in vitro reveals potential impacts of microplastics and nanoplastics on human health: a review. Crit. Rev. Environ. Sci. Technol. 52, 3863–3895. https://doi.org/10.1080/10643389.2021.1951528.

Singh, N., Tiwari, E., Khandewal, N., Darbha, G.K., 2019. Understanding the stability of nanoplastics in aqueous environments: effect of ionic strength, temperature, dissolved organic matter, clay, and heavy metals. Environ. Sci. Nano 6, 2968. https://doi.org/10.1039/c9en00557a.

Strand, S.P., Nordengen, T., Østgaard, K., 2002. Efficiency of chitosans applied for flocculation of different bacteria. Water Res. 36, 4745–4752. https://doi.org/10.1016/S0043-1354(02)00173-2.

Synowiecki, J., Al-Khateeb, N.A., 2003. Production, properties, and some new applications of chitin and its derivatives. Crit. Rev. Food Sci. Nutr. 43, 145–171. https://doi.org/10.1080/10408690390826473.

Tallec, K., Blard, O., González-Fernández, C., Brotons, G., Berchel, M., Soudant, P., Huvet, A., Paul-Pont, I., 2019. Surface functionalization determines behavior of nanoplastic solutions in model aquatic environments. Chemosphere 225, 639–646. https://doi.org/10.1016/j.chemosphere.2019.03.077.

Tang, W., Li, H., Fei, L., Wei, B., Zhou, T., Zhang, H., 2022. The removal of microplastics from water by coagulation: a comprehensive review. Sci. Total Environ. 851, 158224 https://doi.org/10.1016/j.scitotenv.2022.158224.

Venkatesan, J., Bhatnagar, I., Kim, S.K., 2014. Chitosan-alginate biocomposite containing fucoidan for bone tissue engineering. Mar. Drugs 12, 300–316. https://doi.org/10.3390/md12010300.

Wang, X., Li, Y., Zhao, J., Xia, X., Shi, X., Duan, J., Zhang, W., 2020. UV-induced aggregation of polystyrene nanoplastics: effects of radicals, surface functional groups

and electrolyte. Environ. Sci. Nano 7, 3914–3926. https://doi.org/10.1039/d0en00518e.

Wang, Z., Sun, C., Li, F., Chen, L., 2021. Fatigue resistance, re-usable and biodegradable sponge materials from plant protein with rapid water adsorption capacity for microplastics removal. Chem. Eng. J. 415, 129006 https://doi.org/10.1016/j.cej.2021.129006.

Wickramasinghe, S.R., Leong, Y.K., Mondal, S., Liow, J.L., 2010. Influence of cationic flocculant properties on the flocculation of yeast suspensions. Adv. Powder Technol. 21, 374–379. https://doi.org/10.1016/j.apt.2010.02.006.

Wu, J., Jiang, R., Lin, W., Ouyang, G., 2019. Effect of salinity and humic acid on the aggregation and toxicity of polystyrene nanoplastics with different functional groups and charges. Environ. Pollut. 245, 836–843. https://doi.org/10.1016/j.envpol.2018.11.055.

Yang, R., Li, H., Huang, M., Yang, H., Li, A., 2016. A review on chitosan-based flocculants and their applications in water treatment. Water Res. 95, 59–89. https://doi.org/10.1016/j.watres.2016.02.068.

Yao, W., Byrne, R.H., 2001. Spectrophotometric determination of freshwater ph using bromocresol purple and phenol red. Environ. Sci. Technol. 35, 1197–1201. https://doi.org/10.1021/es001573e.

Zhang, F., Wang, Z., Wang, S., Fang, H., Wang, D., 2019. Aquatic behavior and toxicity of polystyrene nanoplastic particles with different functional groups: complex roles of pH, dissolved organic carbon and divalent cations. Chemosphere 228, 195–203. https://doi.org/10.1016/j.chemosphere.2019.04.115.

Zhang, Y., Diehl, A., Lewandowski, A., Gopalakrishnan, K., Baker, T., 2020. Removal efficiency of micro- and nanoplastics (180 nm–125 μm) during drinking water treatment.pdf. Sci. Total Environ. 720, 137383 https://doi.org/10.1016/j.scitotenv.2020.137383.

Zhang, Yunhai, Wang, X., Li, Ying, Wang, H., Shi, Y., Li, Yang, Zhang, Yongjun, 2022. Improving nanoplastic removal by coagulation: impact mechanism of particle size and water chemical conditions. J. Hazard. Mater. 425, 127962 https://doi.org/10.1016/j.jhazmat.2021.127962.

Zheng, B., Li, B., Wan, H., Lin, X., Cai, Y., 2022. Coral-inspired environmental durability aerogels for micron-size plastic particles removal in the aquatic environment. J. Hazard. Mater. 431 https://doi.org/10.1016/j.jhazmat.2022.128611.

Zhou, G., Huang, X., Xu, H., Wang, Q., Wang, M., Wang, Y., Li, Q., Zhang, Y., Ye, Q., Zhang, J., 2022. Removal of polystyrene nanoplastics from water by CuNi carbon material: the role of adsorption. Sci. Total Environ. 820, 153190 https://doi.org/10.1016/j.scitotenv.2022.153190.